Acta Crystallographica Section A
Foundations of Crystallography
ISSN 0108-7673

Received 7 May 2009
Accepted 29 June 2009

Point substitution processes for decagonal quasiperiodic tilings

Nobuhisa Fujita

Institute of Multidisciplinary Research for Advanced Materials, Tohoku University, Sendai 980-8577, Japan. Correspondence e-mail: nobuhisa@tagen.tohoku.ac.jp

A general construction principle for the inflation rules for decagonal quasiperiodic tilings is proposed. The prototiles are confined to be polygons with unit edges. An inflation rule for a tiling is the combination of expansion and division of the tiles, where the expanded tiles can be divided arbitrarily as long as the set of prototiles is maintained. A certain kind of point decoration process turns out to be useful for the identification of possible division rules. The method is capable of generating a broad range of decagonal tilings, many of which are chiral and have atomic surfaces with fractal boundaries. Two new families of decagonal tilings are presented; one is quaternary and the other ternary. The properties of the ternary tilings with rhombic, pentagonal and hexagonal prototiles are investigated in detail.

1. Introduction

Since the discovery of quasicrystals (QCs) (Shechtman *et al.*, 1984), there has been a surge of interest in quasiperiodic tilings with noncrystallographic point symmetries. Archetypes of such tilings in the plane are the Ammann–Beenker tiling (Grünbaum & Shephard, 1987; Beenker, 1982), the Penrose tilings (Grünbaum & Shephard, 1987; Penrose, 1974, 1978, 1979) and the Stampfli square–triangle tilings (Stampfli, 1986; Baake *et al.*, 1992), which belong to the octagonal, decagonal and dodecagonal Bravais classes, respectively. Their vertices form a quasiperiodic point set called a quasilattice (QL), which mimics the spatial arrangement of clusters in a two-dimensional QC. In real QCs, still a far wider variety of cluster arrangements are possible under different compositions and temperatures (Edagawa *et al.*, 1994, 2000). In order to advance our understanding of the real structures, it is therefore necessary to extend our scope for tiling models of QCs and to describe the structures in a more systematic fashion. In the present report, we mean by a two-dimensional tiling *a disjoint covering of the plane by edge-sharing copies of a finite number of polygonal prototiles*.

In general, a two-dimensional QL is constructed as a section of a four-dimensional hypercrystal along the plane (physical space), where the hypercrystal is constructed from atomic surfaces (also called acceptance regions, acceptance domains or windows) arranged periodically according to the relevant Bravais hyperlattice. Each atomic surface extends only along the perpendicular space, which is an orthogonal complement to the physical space. It is the size and the shape of the atomic surface(s) that determine most of the properties of the QL. QLs that are mutually related through a uniform shift along the perpendicular space form the so-called LI class, where LI stands for *local indistinguishability* or *local isomorphism*.[1]

When constructing two-dimensional QLs by the section method, it might seem that atomic surfaces are restricted to be polygonal. However, certain important structures cannot be obtained in this way; the dodecagonal square–triangle tilings are typical examples which have rather complicated fractal atomic surfaces (Stampfli, 1986; Baake *et al.*, 1992; Smith, 1993; Cockayne, 1994). Further examples with fractal atomic surfaces can also be found in the literature (Zobetz, 1992; Godrèche *et al.*, 1993; Cockayne, 1995; Niizeki, 2007*a*). These structures have been discovered by inflation methods, in which the shapes of atomic surfaces are not given *a priori*. It is important to note that even for a known atomic surface with a fractal boundary, the computation of the structure by the section method is impractical because minute numerical errors cannot be avoided in judging which side of the boundary lies a given point near the boundary. Therefore, the section method does not suit the generation of such a QL, whereas an inflation method can work well.

So far, a systematic attempt has been made to generate one-dimensional binary tilings by inflation rules (Luck *et al.*, 1993), revealing that the structures tend to have fractal (Cantor-set-like) atomic surfaces. In more than two dimensions, however, inflation rules for quasiperiodic tilings are rarely known, except for those described above. This situation is simply caused by the difficulty in finding an inflation rule that does not produce any inconsistency throughout the entire structure. There is nevertheless some hope at present. Recently, a systematic inflation method was developed for generating QLs, *i.e.* quasiperiodic point sets, in general dimensions (Niizeki, 2008). Let us call this method the *point inflation scheme* (PIS) and each of its inflation algorithms a *point inflation rule* (PIR). At this point, however, it should be

[1] LI classes of QLs are further grouped into mutual-local-derivability classes (Baake *et al.*, 1991; Baake & Schlottmann, 1997).

remembered that a QL does not necessarily provide the vertices of a tiling.

An advantage of employing tiling models for QCs lies in the fact that they enable the entire structure to be decomposed into a finite number of *prototiles*, or fundamental structural units. Another possible advantage may lie in their stronger geometrical constraints, which are based on physical reasoning such as the avoidance of unrealistic short distances. The present aim is therefore to develop a new inflation scheme for generating quasiperiodic tilings. As in the case of archetypal tilings in the plane, inflation rules should proceed by the following steps: (1) expansion of the tiling and (2) division of the expanded tiles into tiles of the original size. Bear in mind that the expanded tiles can be divided in an arbitrary way as long as the set of prototiles is maintained.

Here we propose to generalize the division of the tiles with the help of a point decoration process. The point decoration might simply be defined by a PIR, but this cannot prevent excess points from being generated in general. One needs to remove a part of the resulting point set so that the remaining points constitute the vertex set of a tiling. Wherefore, the point decoration can be defined instead by taking an appropriate subset of the set generated by a PIR. In other words, the PIR is used to obtain the candidate positions for the decoration, then only a part of it is accepted. The present scheme turns out to be useful for discovering unknown tilings. For the sake of a self-contained presentation, the following arguments are confined to the decagonal case. Furthermore, the edges of any tiling to be considered are all given by one of the ten unit vectors, $\mathbf{e}_j$ ($j = 0, \ldots, 9$), which will be defined in §2.

The decagonal Bravais module $\mathbf{\Lambda}_{10}$ is introduced in §2, which is devoted to mathematical preliminaries. It is a projection of the four-dimensional decagonal lattice onto the two-dimensional physical space. The new scheme for generating decagonal tilings is presented in §3. In §4, the present scheme is applied to obtain two new families of decagonal tilings; one is quaternary and the other ternary. The atomic surfaces of the new tilings are presented in §5. In particular, for the ternary tilings the atomic surfaces with fractal boundaries are derived geometrically as the fixed sets of the dual maps associated with the relevant inflation rules. A statistical analysis is performed for the ternary tilings in §6. Further remarks are given in §7.

2. Decagonal Bravais module

Let us define the quasicrystallographic axes for a decagonal QL by the ten unit vectors $\mathbf{e}_j = (\cos(j\theta), \sin(j\theta))$ with $j = 0, 1, 2, \ldots, 9$ and $\theta = \pi/5$, pointing at the vertices of a regular decagon centred at the origin. Among the ten vectors, only four are linearly independent with respect to integer coefficients. A conventional set of basis vectors is introduced as $\tilde{\mathbf{e}}_j := \mathbf{e}_{2j}$ ($j = 0, 1, 2, 3$), pointing at four vertices of a pentagon from the origin, where the fifth vertex $\tilde{\mathbf{e}}_4 := \mathbf{e}_8$ is left unused because it can be represented by the four bases; $\tilde{\mathbf{e}}_4 = -\sum_{j=0}^{3} \tilde{\mathbf{e}}_j$. The basis set generates a Z-module of rank four called the decagonal Bravais module, denoted by the symbol $\mathbf{\Lambda}_{10}$. Remember that the point group of $\mathbf{\Lambda}_{10}$ is the dihedral group D_{10} (or 10*mm* in Hermann–Mauguin notation). Furthermore, $\mathbf{\Lambda}_{10}$ has an important property of scaling invariance $\tau\mathbf{\Lambda}_{10} = \mathbf{\Lambda}_{10}$, where $\tau = (1 + \sqrt{5})/2$ is the golden mean (Niizeki, 1989*a*).[2]

The decagonal Bravais hyperlattice $\boldsymbol{L}_{10}$ is defined in a four-dimensional Euclidean hyperspace $\mathbb{E}_4$, and it is generated by the primitive basis vectors $(\tilde{\mathbf{e}}_j, \xi\tilde{\mathbf{e}}_j^{\perp})$ (j = 0, 1, 2 and 3), where $\tilde{\mathbf{e}}_j^{\perp} := \mathbf{e}_{4j\,(\mathrm{mod}\,10)}$ (Niizeki, 1989*a*; Yamamoto, 1996) and ξ is an arbitrary scale factor satisfying $0 < \xi \neq 1$. The point group G of $\boldsymbol{L}_{10}$ is isomorphic to the dihedral group D_{10}. The two-dimensional physical space $\mathbb{E}^{\parallel}$ is an irreducible subspace of $\mathbb{E}_4$ with respect to G, and it is inclined against $\boldsymbol{L}_{10}$ in an incommensurate fashion. The orthogonal projection of $\boldsymbol{L}_{10}$ onto $\mathbb{E}^{\parallel}$ gives nothing but the decagonal Bravais module $\mathbf{\Lambda}_{10}$.

The two-dimensional perpendicular space $\mathbb{E}^{\perp}$ is defined as the orthogonal complement to $\mathbb{E}^{\parallel}$ in $\mathbb{E}_4$; that is, $\mathbb{E}_4 = \mathbb{E}^{\parallel} \oplus \mathbb{E}^{\perp}$. Then the hyperlattice $\boldsymbol{L}_{10}$ can be projected onto $\mathbb{E}^{\perp}$ as well, generating another Z-module, $\mathbf{\Lambda}_{10}^{\perp}$. Since the orthogonal projections from $\boldsymbol{L}_{10}$ to both $\mathbf{\Lambda}_{10}$ and $\mathbf{\Lambda}_{10}^{\perp}$ are bijections, one can introduce a natural bijection $\hat{\boldsymbol{\pi}}$ between the Z-modules; $\mathbf{\Lambda}_{10}^{\perp} = \hat{\boldsymbol{\pi}}\mathbf{\Lambda}_{10}$.

We confine ourselves to the case when the vertex set $\mathbf{\Sigma}_{\mathcal{T}}$ of a tiling $\mathcal{T}$ is a subset of the Bravais module $\mathbf{\Lambda}_{10}$. In the ordinary cut-and-projection method (de Bruijn, 1981; Mackay, 1982; Kramer & Neri, 1984; Duneau & Katz, 1985), $\mathbf{\Sigma}_{\mathcal{T}}$ is generated as the orthogonal projection of $(\mathbb{E}^{\parallel} + \boldsymbol{W}) \cap \boldsymbol{L}_{10}$, a cut of $\boldsymbol{L}_{10}$ within a strip along $\mathbb{E}^{\parallel}$, onto $\mathbb{E}^{\parallel}$. The cross section of the strip, $\boldsymbol{W}(\subset \mathbb{E}^{\perp})$, is equivalent to the atomic surface in the section method. The image of $\mathbf{\Sigma}_{\mathcal{T}}$ in $\mathbb{E}^{\perp}$ is denoted as $\mathbf{\Sigma}_{\mathcal{T}}^{\perp} := \hat{\boldsymbol{\pi}}\mathbf{\Sigma}_{\mathcal{T}}$. In general, $\mathbf{\Sigma}_{\mathcal{T}}^{\perp}$ is a dense subset of the atomic surface $\boldsymbol{W}$, which on the other hand should be included in the closure of $\mathbf{\Sigma}_{\mathcal{T}}^{\perp}$, *i.e.* $\mathbf{\Sigma}_{\mathcal{T}}^{\perp} \subset \boldsymbol{W} \subseteq \overline{\mathbf{\Sigma}_{\mathcal{T}}^{\perp}}$.[3]

3. Generalized point substitution processes for tilings

In the PIS (Niizeki, 2008), a PIR is formulated as a set map φ that acts on an arbitrary subset $\boldsymbol{L}$ of $\mathbf{\Lambda}_{10}$. φ proceeds by expanding $\boldsymbol{L}$ by a certain ratio σ (>1) and subsequently placing a copy of a certain motif $\boldsymbol{S}(\subset \mathbf{\Lambda}_{10})$ centred at every vertex. The ratio σ can take any natural power of the Pisot unit τ (the golden mean) associated with $\mathbf{\Lambda}_{10}$, so that $\sigma\boldsymbol{L}$ remains a subset of $\mathbf{\Lambda}_{10}$. The motif $\boldsymbol{S}$ is a bounded set with a finite number of points comprised of one or more shells, each of which is an orbit of a point with respect to the point group D_{10}. One can put the procedure in a simple form as $\varphi(\boldsymbol{L}) := \sigma\boldsymbol{L} + \boldsymbol{S}$, in which the $+$ symbol implies $\boldsymbol{A} + \boldsymbol{B} \equiv \{a + b \mid^{\forall} a \in \boldsymbol{A}, {}^{\forall} b \in \boldsymbol{B}\}$. Note that the resultant QL would have the point group D_{10}.

[2] In general, the ratio τ is called the Pisot unit in the algebraic theory of Bravais modules. For the octagonal or the dodecagonal cases, it takes the value $1 + \sqrt{2}$ or $2 + \sqrt{3}$, respectively.

[3] Some authors (Baake *et al.*, 1991; Niizeki, 2008) define an atomic surface $\boldsymbol{W}$ as a compact (*i.e.*, closed and bounded) set in $\mathbb{E}^{\perp}$, hence $\boldsymbol{W} = \overline{\mathbf{\Sigma}_{\mathcal{T}}^{\perp}}$. In this paper, however, a more general approach is taken so that a part of the boundary $\partial\boldsymbol{W}$ may be absent from $\boldsymbol{W}$ while fulfilling the gluing condition, as explained in the text for the case of the RPH tilings (see Fig. 8).

The atomic surface of a QL generated by the PIS is identified as the unique attractor (Hutchinson, 1981) of the dual set map $\varphi^{\perp}$ that acts in the perpendicular space; $\varphi^{\perp}(\boldsymbol{X}) := \sigma^{*}\boldsymbol{X} + \boldsymbol{S}^{\perp}$, where σ^{*} denotes the algebraic conjugate of σ, $\boldsymbol{X}$ an arbitrary set in $\mathbb{E}^{\perp}$ and $\boldsymbol{S}^{\perp} = \hat{\boldsymbol{\pi}}\boldsymbol{S}$. The dual set map $\varphi^{\perp}$ is contractive since $0 < |\sigma^{*}| < 1$; it is nothing but an iterated function system (IFS), which is a common technique for generating fractal objects (Falconer, 1990). Indeed, the atomic surfaces of many QLs generated by the PIS have fractal boundaries. Various planar QLs have been found by the PIS (Niizeki, 2008), which has also been applied to the case of icosahedral QLs (Fujita & Niizeki, 2008).

Certain QLs can produce a tiling if the points are connected by uncrossed edges of unit length, where the tiles are the regions bounded by these edges. Let us call this property the *unit connectivity* (UC) of the point sets. If a point set obtained by successively applying a PIR has the UC property, the PIR can be translated into an inflation rule for the tiling; that is, expansion of the tiles followed by their division into the original tiles. The division rules of the tiles are determined by the generated points in the tiles. In general, however, undesirable short distances prevent the generated point sets from being translated into tilings. Such redundancies can be discarded only by introducing an elimination step at each iteration to take an appropriate subset which fulfils the UC property. Then the expanded tiles are divided properly. We call the new inflation process a generalized point substitution process (GPSP). In the GPSP, the role of the PIR is to generate the *candidate positions for the vertices of a tiling*.

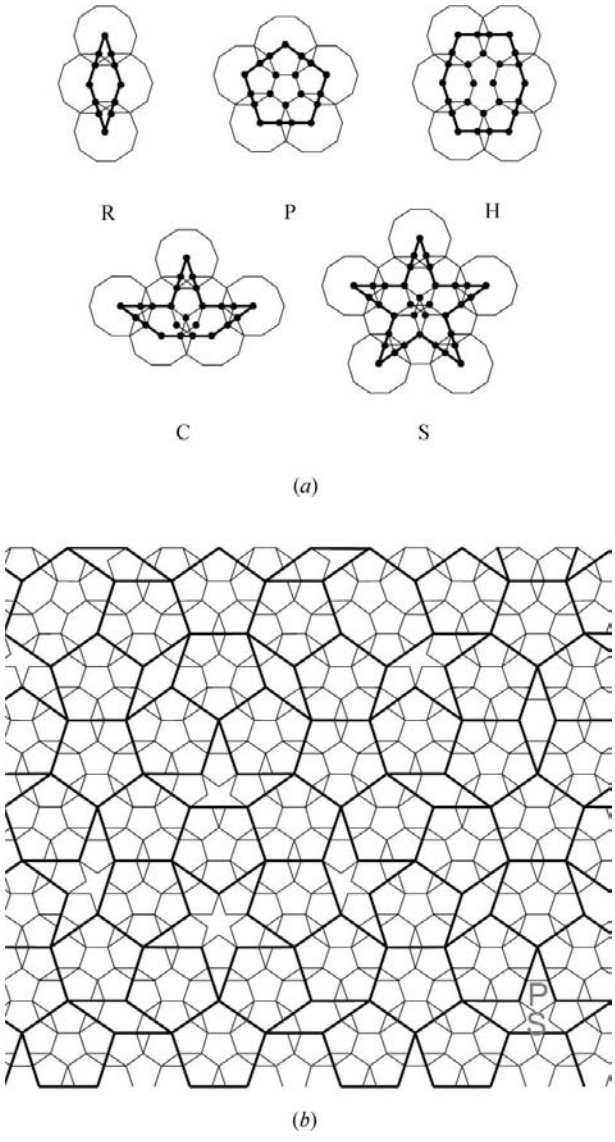

Figure 1
(*a*) The point decorations of the expanded prototiles for the *para*-Penrose tiling are determined by superposing decagons centred at all the vertices. (*b*) A square patch of the *para*-Penrose tiling with expanded tiles being indicated by the thicker lines shows the division rules for the expanded tiles. An S–P complex is indicated in the bottom-right corner.

For now, the UC property is required by the point set at every iteration of a GPSP. A GPSP for decagonal tilings is formally given by the following steps: Step I is expansion of the tiling by the ratio σ, where σ is a natural power of τ (the golden mean), and step II is the decoration of every expanded tile by points, where the positions of the points should originate from $\boldsymbol{\Lambda}_{10}$ and are assumed to be determined uniquely by the shape of the expanded tile as well as those of its adjacent neighbours. In practice, candidate positions for the points of decoration are generated by a PIR, then an appropriate subset is taken to determine the division of the tiles. Note that there are degrees of freedom for the choice of the point decoration provided that the point decoration is determined uniquely within the first adjacent neighbours and that the set of prototiles is maintained. It is this generality that allows us to produce a broad class of new quasiperiodic tilings. The degrees of freedom can be promoted further by allowing the decoration to depend on farther neighbours. However, this would complicate the algorithm and will not be considered.

4. Examples of decagonal tilings

Several decagonal tilings are generated by the GPSP scheme. All the tilings presented below obey the UC property, in which the vertices are connected through the ten unit vectors $\mathbf{e}_j$ ($j = 0, \ldots, 9$) that form the edges of the tiles. Any vertex can therefore be written as $\mathbf{l} = n_0\tilde{\mathbf{e}}_0 + n_1\tilde{\mathbf{e}}_1 + n_2\tilde{\mathbf{e}}_2 + n_3\tilde{\mathbf{e}}_3$, or alternatively it can be indexed as $\mathbf{l} = [n_0n_1n_2n_3]$.

4.1. *para*-Penrose tiling

The present tiling has been reported already (Niizeki, 2008) as one of the simplest decagonal tilings that can be generated by the PIS. The scaling ratio of the relevant PIR is $\sigma = \tau^2$, while the motif $\boldsymbol{S}$ consists of two shells $\langle[0000]\rangle$ and $\langle[1100]\rangle$, where $\langle\mathbf{l}\rangle := \{g\mathbf{l} \mid g \in D_{10}\}$ is the orbit of the point $\mathbf{l}$ with respect to D_{10}. In addition to the four prototiles, *i.e.*, the 36° rhombus (R), the regular pentagon (P), the crown (C) and the pentacle star (S) of the pentagonal Penrose tiling (P1) (Penrose, 1974; Grünbaum & Shephard, 1987), it has another prototile, namely the barrel-shaped hexagon (H). This tiling is called the *para*-Penrose tiling by Niizeki (2008).

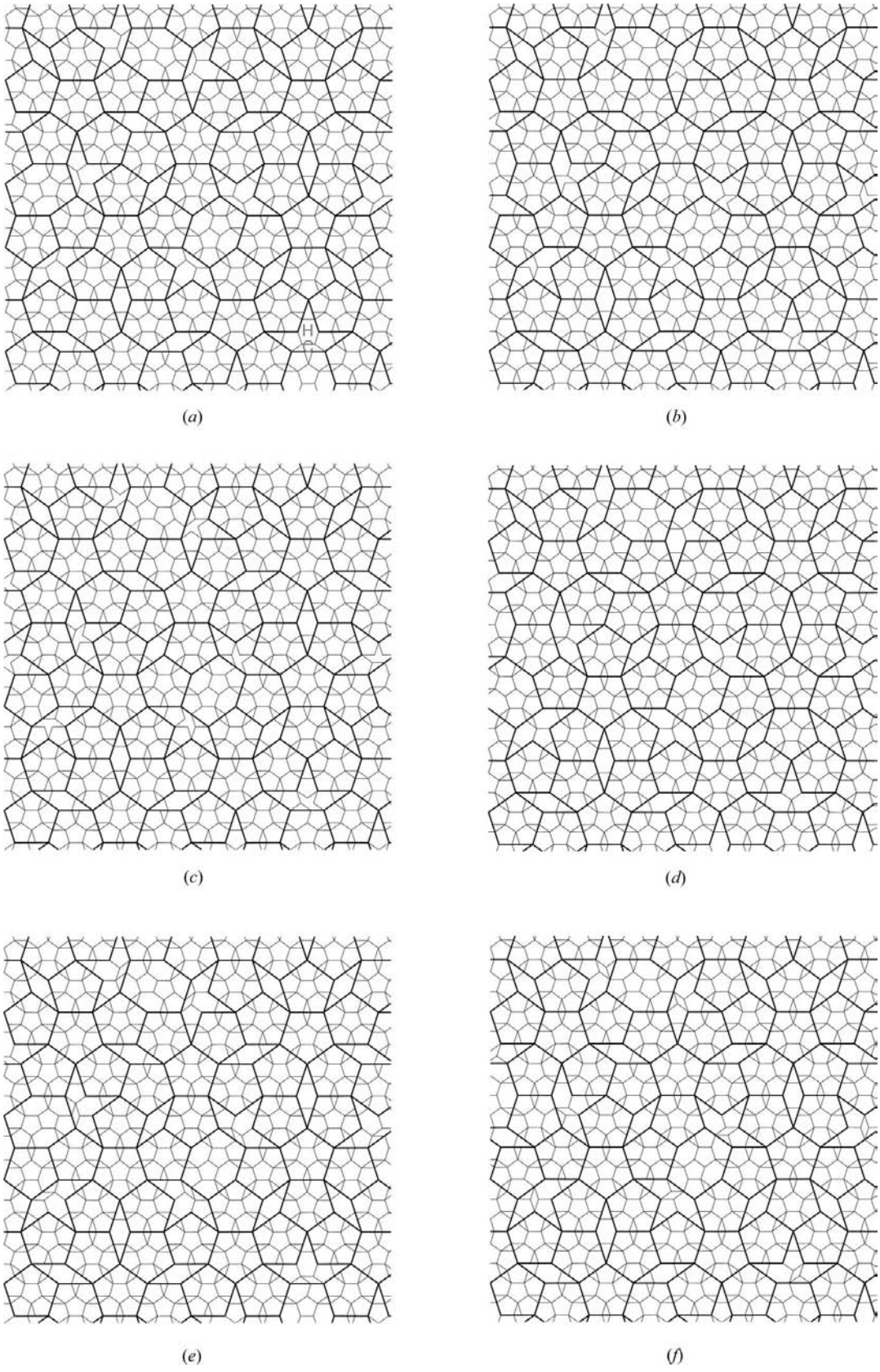

Figure 2
Square patches of RPHC tilings generated by GPSPs with expanded tiles being indicated by the thicker lines. They are distinguished by the division of the G complex lying on the bottom of every expanded C tile. The division rules of the expanded P and H tiles are also affected by adjacent C tiles. (*a*–*c*) A single point inside every G complex is eliminated, while the mirror symmetry is retained only in (*a*). A C–H complex is indicated in the bottom-right corner of (*a*). (*d*–*e*) Two internal points of every G complex are eliminated. The mirror symmetry is retained only in (*d*).

In a single iteration, these tiles are expanded by the ratio τ^2 and then a copy of $\boldsymbol{S}$ is placed on every vertex; see Fig. 1(*a*). One finds that each expanded tile is uniquely decorated with the points of $\boldsymbol{S}$'s within its border. As the new points are connected with unit edges, the expanded tile is divided into tiles of the original size, whereas in the vicinity of the boundary the tiles can be shared with the neighbouring expanded tiles. In particular, when dividing an expanded P or H tile, segments near the boundary can be attributed to different kinds of tiles. This means that the division rule is not unique within the expanded tile itself. Still, it turns out to be unique within the first adjacent neighbours, as one can readily check in Fig. 1(*b*). Therefore, the present PIR satisfies the necessary conditions for a GPSP.

4.2. RPHC tilings

The PIR for the *para*-Penrose tiling can be slightly altered by removing a generated vertex inside every expanded C tile at the symmetrical position. Obviously this does not affect the uniqueness of the decoration within every expanded prototile, and the resulting point set is shown to satisfy the UC property. As a consequence, the combination of an S tile and a P tile (S–P complex) lying at the centre of every expanded C tile turns into one of a C tile and an H tile (C–H complex); see the labelled pairs in the bottom-right corners of Figs. 1(*b*) and 2(*a*). Since the S prototile may no longer appear except at the centre of an expanded S tile, it is a marginal one in the present case; that is, an iteration of the above GPSP will generate a quaternary tiling with R, P, H and C prototiles as shown in Fig. 2(*a*). The division rule of every expanded tile depends on its first adjacent neighbours, as in the case of the *para*-Penrose tiling.

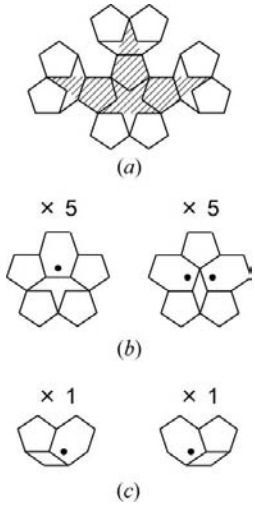

Figure 3
(*a*) One G and three T complexes associated with an expanded C tile (the hatched area) are shown. (*b*) Depending on whether one or two internal vertices are removed, a G complex is divided in two different ways, which may further take five distinct orientations relative to the expanded C tile. (*c*) A T complex can be divided in two ways depending on the choice of an internal vertex to be removed. In (*b*) and (*c*), the black dots indicate the removed vertices.

There are yet different ways to remove a vertex in an expanded C tile without affecting the set of prototiles. Let us consider a gear-shaped complex (or a G complex), formed by an S tile at the centre and five adjacent P tiles (see Fig. 3*a*), lying on the bottom of the expanded C tile. Either one or two of its five internal vertices may be removed. Thus the G complex may be divided in two ways. By removing one vertex, the G complex is divided into one H, one C and four P tiles (Fig. 3*b*, left). There are five possible orientations, one of which has been taken in the preceding paragraph. Two other orientations are used in Fig. 2(*b*) and (*c*), while the remaining two are their mirror images. Removing two internal vertices affords yet another way to divide the G complex (Fig. 3*b*, right). Of the five possible orientations, the only one that does not break the mirror symmetry is used in Fig. 2(*d*). Two other choices are shown in Fig. 2(*e*) and (*f*), while the remaining two are their mirror images. By removing two vertices, the G complex is divided into one R, two H and three P tiles.

We have constructed in total ten GPSPs for tilings with the identical set of four prototiles. Recall that the eight GPSPs without mirror symmetry would generate chiral tilings. If the ten GPSPs are applied in a mixed and arbitrary order, infinitely many tilings can be generated. Furthermore, if different GPSPs are allowed to be applied at different locations at the same time, the possibilities become unlimited.

4.3. RPH tilings

Let us see how the C prototile can be excluded from the prototiles of RPHC tilings. Consider a turban-shaped complex (or a T complex) composed of a C tile and two adjacent P tiles in an RPHC tiling. A T complex is associated to every 36° angle of the expanded R and C tiles. The T complex can be decomposed into three tiles, R, P and H tiles, by removing one of the two inner vertices, thereby breaking the mirror symmetry; see Fig. 3(*c*). If all the T complexes are (re-)divided in such a way, an RPHC tiling turns into a tiling which does not include any C tile. The two different ways to divide the T complex are mirror images of one another, thus *left*- and *right*-handed chiralities are associated with them.

It is tempting to apply either one of the chiral rules for dividing all the T complexes; then the two GPSPs for both chiralities are obtained. These GPSPs maintain the set of the prototiles, R, P and H. The left-handed GPSP is shown in Fig. 4, the repetition of which generates a tiling shown in Fig. 5(*a*). The mirror images of these figures correspond to the right-handed counterparts. Note that the point decorations within the expanded prototiles are not uniquely determined in this case, but they are unique within the first adjacent shell. The decoration uniquely determines the division of the expanded prototiles. The two GPSPs may be applied in an arbitrary order, resulting in an infinite number of RPH tilings. A tiling shown in Fig. 5(*b*) is an outcome of an alternate repetition of the right- and the left-handed GPSPs, where the final GPSP is the left-handed one. In both of the tilings shown in Fig. 5, a spiral pattern associated with the left-handed chirality can be easily recognized. Again, many more possibilities exist if the

two GPSPs are allowed to be applied at different locations at the same time.

5. Atomic surfaces

The atomic surface of a quasiperiodic tiling $\mathcal{T}$ is closely connected with the global characteristics of the structure. It can be inferred by projecting the vertices of a patch of $\mathcal{T}$ containing a sufficient number of vertices onto the perpendicular space, $\mathbb{E}^{\perp}$. This is done in Fig. 6 for the six RPHC tilings and in Fig. 7 for the two RPH tilings. The convex hulls of all these atomic surfaces are the regular decagon whose vertices are given by $\xi\mathbf{e}_j$ $(j = 0, \ldots, 9)$, corresponding to the atomic surface of the Penrose P1 tiling. However, different types of erosion are observed near the boundaries even for tilings with the same set of prototiles. The symmetry of an atomic surface reflects that of the relevant tiling; all the atomic surfaces except the two with the mirror symmetric GPSPs (Figs. 6*a* and *d*) have the lower point symmetry with the cyclic group C_{10} (or 10). For each case, the erosion reveals complicated fractal patterns. In particular, the three atomic surfaces that are shown in Figs. 6(*a*), (*c*) and (*e*) exhibit hierarchical holes in the boundary regions. The rest of the atomic surfaces maintain the disc-like topology.

Recall that for a QL generated by the PIS the atomic surface is simply identified as the unique attractor of the dual set map $\varphi^{\perp}(\boldsymbol{X}) = \sigma^{*}\boldsymbol{X} + \boldsymbol{S}^{\perp}$ (Niizeki, 2008); see §3. For a tiling generated by the GPSP scheme, on the other hand, the dual set map is associated with the determination of the candidate positions, from which a certain subset should be eliminated.

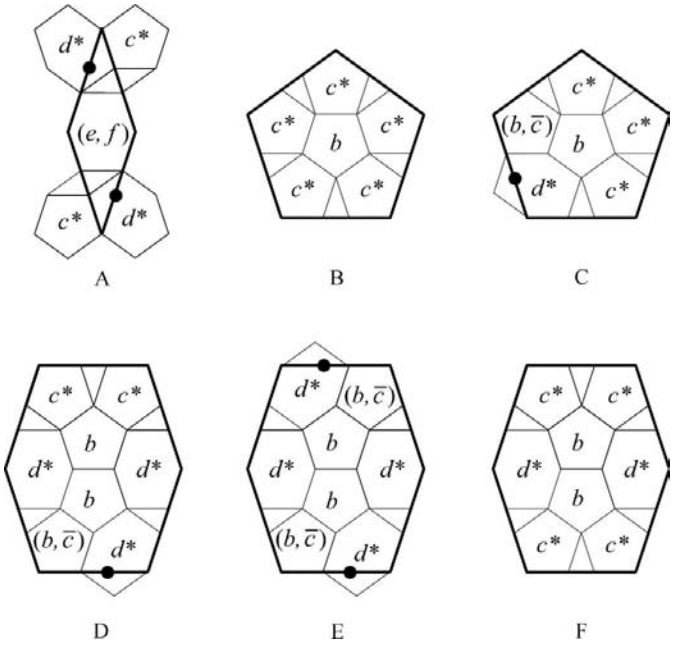

Figure 4
The left-handed GPSP for the RPH tilings is shown. An expanded P or H tile is divided in several different ways depending on its first adjacent neighbours. Expanded tiles are thus classified into six classes according to their division rules; they are labelled A to F. The black dots indicate the removed vertices inside T complexes. The generated tiles can also be classified into six classes but in two different ways depending on the chirality of the subsequent GPSP (see also §6). For instance, a P tile labelled $(b, \overline{c})$ implies that it is classified into the b subclass if the next GPSP is left-handed while into the $\overline{c}$ subclass if the next GPSP is right-handed, where the bar indicates the mirror reflection. A mutually inverted pair is denoted by a starred label; that is, $c^{*} = (c, \overline{c})$ and $d^{*} = (d, \overline{d})$. The label a^{*} [*i.e.* $(a, \overline{a})$] for each R tile is suppressed merely for the reason of space. Tiles with the label f only appear if the two successive GPSPs have opposite chiralities, while tiles with the label e (or $\overline{e}$) only appear if the same GPSP is applied successively.

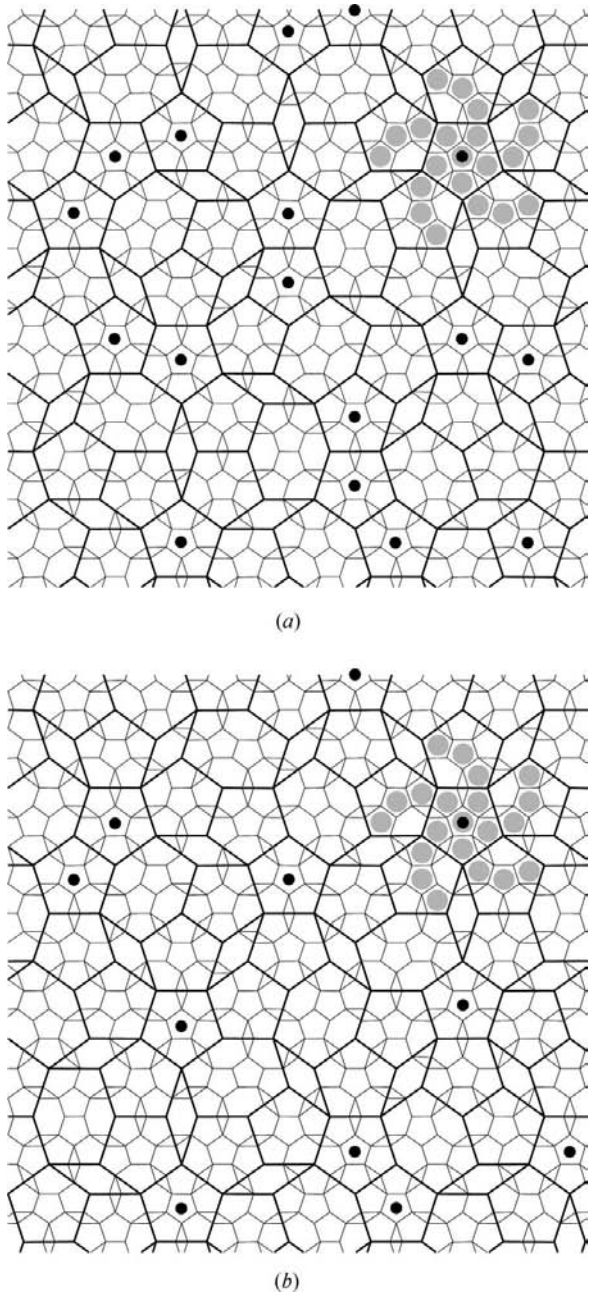

Figure 5
Square patches of RPH tilings generated by repeating the left-handed GPSP (*a*) and by alternating between the right- and left-handed GPSPs (*b*). Spirals in the arrangement of P tiles are emphasized with grey spots. The black dots indicate the centres of the expanded P tiles with the fivefold symmetric division rule (Fig. 4, B), showing that the frequencies of local fivefold centres are somewhat different between the two.

The elimination is represented in $\mathbb{E}^{\perp}$ as a subtraction of unnecessary parts from $\varphi^{\perp}(\boldsymbol{X})$. In the following, the latter process is presented for the RPH tilings, in which case geometrical rules to determine the atomic surfaces are identified. However, since such geometrical rules are not easy to generalize, the case of the RPHC tilings will be left open.

The PIR for the *para*-Penrose tiling given in §4.1 gives $\boldsymbol{S}^{\perp} = \{\langle[0000]\rangle, \langle[1010]\rangle\}$ and $\sigma^{*} = \tau^{-2}$ for the dual set map $\varphi^{\perp}$. The fixed set of $\varphi^{\perp}$, which is a moth-eaten version of the regular decagon (Niizeki, 2008), is the corresponding atomic surface. The small part that is left out from the decagonal atomic surface corresponds to a portion of concave vertices of C tiles and S tiles, resulting in the emergence of H tiles in the *para*-Penrose tiling.

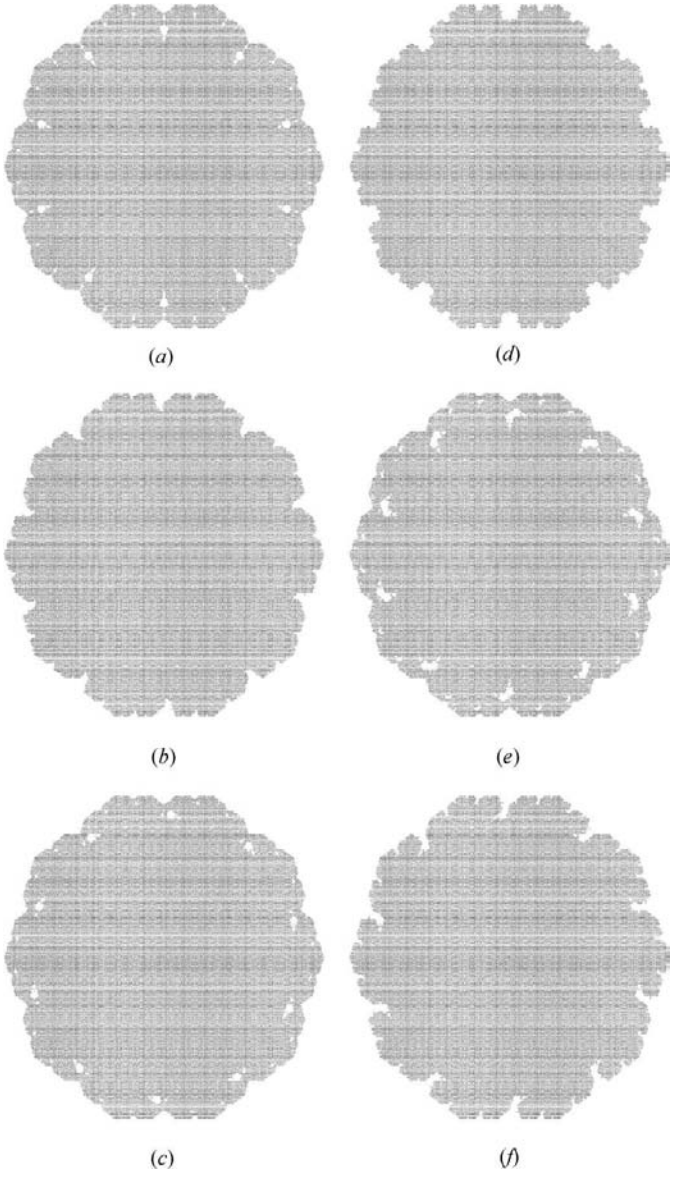

Figure 6
Parts (*a*–*f*) show the atomic surfaces for the RPHC tilings in Figs. 2(*a*–*f*), respectively. The grey areas represent the projections of a large patch containing over 250 000 vertices onto $\mathbb{E}^{\perp}$. Fine details including hierarchical holes (pits) are visible.

In order to obtain the atomic surfaces for the RPH tilings, a subtraction process must be combined with the dual set map at each iteration. In Fig. 8, the initial polygon $\boldsymbol{X}_0$ is defined as a decagonal star, which is known to be the atomic surface of a non-chiral RPH tiling (Papadopolos & Kasner, 2003). It is transformed by the dual set map to $\tilde{\boldsymbol{X}}_0 = \varphi^{\perp}(\boldsymbol{X}_0)$. The subtraction process for the chiral GPSPs (§4.3) can be understood as a carving process near the boundary of $\tilde{\boldsymbol{X}}_0$. Note that five strips are superposed on the next figure, while five more strips can be superposed upside down but are suppressed. These strips are cut by the boundary of $\tilde{\boldsymbol{X}}_0$, while the two ends of each strip do not coincide through a translation. Accordingly, within each cut of the strips, two points can lie on a line parallel to the strip with the distance $\xi\tau$. This leads to an excessive appearance of short distance $1/\tau$ in $\mathbb{E}^{\parallel}$ and hence to the existence of C tiles. It turns out that for an RPH tiling no such pair of points is allowed to exist within a single strip. Therefore, either or both ends of each cut must be carved so that they coincide through $\xi\tau$ translations.

The carving process for the left- or right-handed GPSP is simply to carve a single end only. As shown in Fig. 8, five strips are arranged to form a pentacle star, which can be traced either clockwise or anticlockwise. Let us fix that the pentacle should be traced clockwise. Then for the left-handed GPSP, the first end of each strip encountered while tracing the pentacle should be carved so that it coincides with the translate of the second end. These two ends fulfil the gluing condition; namely, if a point on one end is taken into account, the corresponding point on the other end should be discarded. The carving process for all the ten strips results in a new polygon $\boldsymbol{X}_1$, which is the atomic surface of another RPH tiling (chiral in this case). The carving process is denoted as γ_l, while the right-handed counterpart is denoted as γ_r, in which case the opposite end of each strip is to be carved.

The atomic surface of an RPH tiling generated by the GPSP scheme can be obtained by repeatedly applying $\gamma_l \cdot \varphi^{\perp}$ and/or $\gamma_r \cdot \varphi^{\perp}$. In the example shown in Fig. 8, only the left-handed process $\gamma_l \cdot \varphi^{\perp}$ is used. In general, the subtraction process γ associated with the removal of unnecessary points from the candidate positions can be rather complicated. At present, we have been able to identify γ only for the chiral RPH tilings and some of their variants.[4]

6. Statistics of the RPH tilings

The inflation matrices are introduced in the following to analyse the statistics of the RPH tilings. For each chirality, there are six types of tiles that are divided differently, as can be seen in Fig. 4. In order to define the inflation matrix, the generated tiles need to be classified further into six types, so that their numbers can be counted in each expanded tile. Note, however, that the latter task depends on which chirality is to be used in the next iteration. In Fig. 4, some of the small tiles

[4] Deterministic rules are also found for assigning opposite chiralities to the two T complexes associated with each expanded R tile. This allows us to generate another family of RPH tilings whose point group is D_5 (or $5m$), as will be presented elsewhere.

are assigned different letters according to the chirality of the next GPSP. There are four pairs of chiralities for the two successive iterations, *ll*, *rl*, *lr* and *rr*. It is sufficient to consider two particular cases, *ll* and *rl*, since the other cases are merely mirror images of the former two; the latter have the same inflation matrices as the former.

In the case *ll*, the division rules shown in Fig. 4 reveal that the six expanded tiles are divided as

$$\begin{aligned}
V_A &= V_a + (1/\tau^2)V_d + V_e,\\
V_B &= (5/2)V_a + V_b + 5V_c,\\
V_C &= 2V_a + 2V_b + 3V_c + [1 - (1/2\tau^2)]V_d,\\
V_D &= (5/2)V_a + 3V_b + 2V_c + [3 - (1/2\tau^2)]V_d,\\
V_E &= 2V_a + 4V_b + [4 - (1/\tau^2)]V_d,\\
V_F &= 3V_a + 2V_b + 4V_c + 2V_d,
\end{aligned} \tag{1}$$

where V_x represents the volume of the tile labelled x. In the case *lr*, the corresponding formulae are

$$\begin{aligned}
V_A &= V_{\bar{a}} + (1/\tau^2)V_{\bar{d}} + V_f,\\
V_B &= (5/2)V_{\bar{a}} + V_b + 5V_{\bar{c}},\\
V_C &= 2V_{\bar{a}} + V_b + 4V_{\bar{c}} + [1 - (1/2\tau^2)]V_{\bar{d}},\\
V_D &= (5/2)V_{\bar{a}} + 2V_b + 3V_{\bar{c}} + [3 - (1/2\tau^2)]V_{\bar{d}},\\
V_E &= 2V_{\bar{a}} + 2V_b + 2V_{\bar{c}} + [4 - (1/\tau^2)]V_{\bar{d}},\\
V_F &= 3V_{\bar{a}} + 2V_b + 4V_{\bar{c}} + 2V_{\bar{d}}.
\end{aligned} \tag{2}$$

It follows that the inflation matrices for all the four cases are given by

$$\mathbf{M}_1 := \mathbf{M}_{ll} = \mathbf{M}_{rr} = \begin{pmatrix} 1 & 0 & 0 & 1/\tau^2 & 1 & 0\\ 5/2 & 1 & 5 & 0 & 0 & 0\\ 2 & 2 & 3 & [1-(1/2\tau^2)] & 0 & 0\\ 5/2 & 3 & 2 & [3-(1/2\tau^2)] & 0 & 0\\ 2 & 4 & 0 & [4-(1/\tau^2)] & 0 & 0\\ 3 & 2 & 4 & 2 & 0 & 0 \end{pmatrix} \tag{3}$$

and

$$\mathbf{M}_2 := \mathbf{M}_{lr} = \mathbf{M}_{rl} = \begin{pmatrix} 1 & 0 & 0 & 1/\tau^2 & 0 & 1\\ 5/2 & 1 & 5 & 0 & 0 & 0\\ 2 & 1 & 4 & [1-(1/2\tau^2)] & 0 & 0\\ 5/2 & 2 & 3 & [3-(1/2\tau^2)] & 0 & 0\\ 2 & 2 & 2 & [4-(1/\tau^2)] & 0 & 0\\ 3 & 2 & 4 & 2 & 0 & 0 \end{pmatrix}. \tag{4}$$

One can check that the maximal eigenvalues of both $\mathbf{M}_1$ and $\mathbf{M}_2$ are τ^4, corresponding to the rate of volume increase under

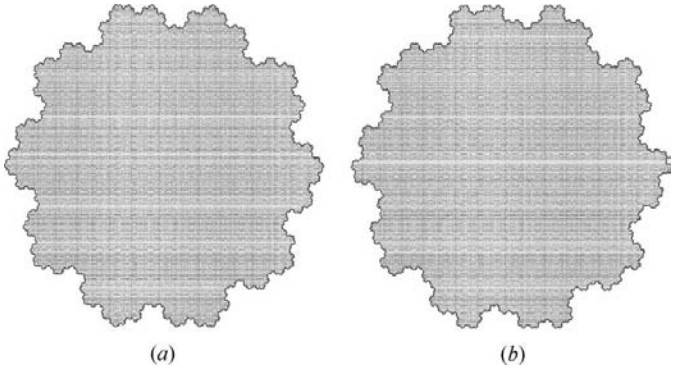

Figure 7
Parts (*a*) and (*b*) show the atomic surfaces for the RPH tilings in Figs. 5(*a*) and (*b*), respectively. The grey areas represent the projections of a large patch containing over 240 000 vertices onto $\mathbb{E}^{\perp}$, while the boundary lines are obtained with the geometrical rules as presented in Fig. 8.

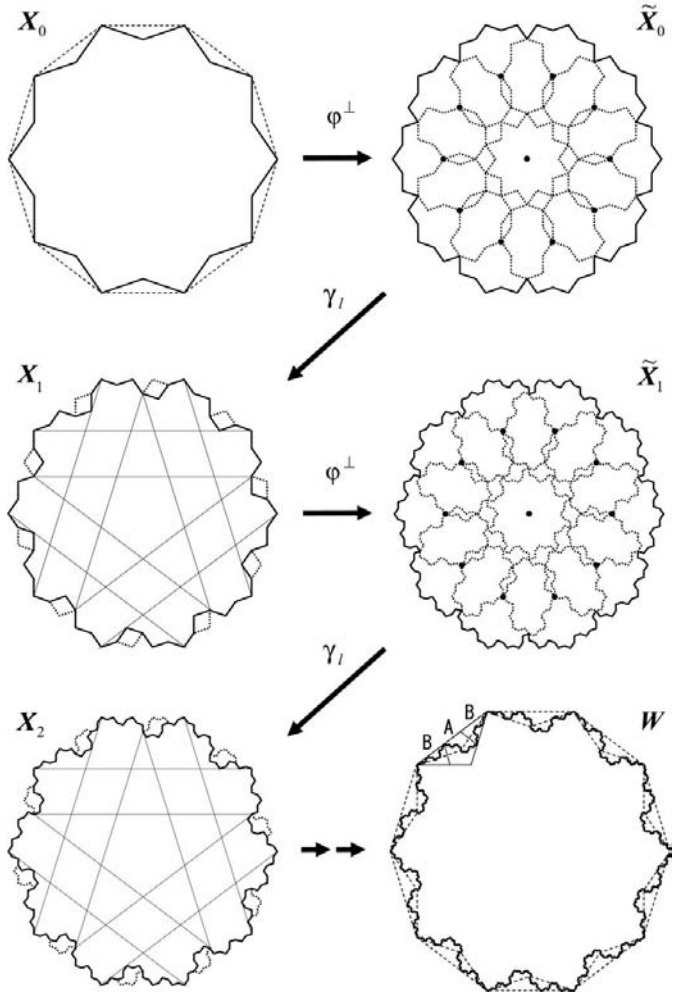

Figure 8
The dual map for the left-handed GPSP is illustrated. Starting from a star decagon $\boldsymbol{X}_0$ for a non-chiral RPH tiling, the dual set map $\varphi^{\perp}$ and the subtraction process γ_l are alternately applied. For applying the dual set map, a copy of the reduced figure, *e.g.* $\sigma^*\boldsymbol{X}_0$, is placed on every point of $\boldsymbol{S}^{\perp}$ indicated by the black dots. For γ_l, a single end of all the ten strips is carved as described in the text. Only five strips are depicted by the thin lines. By iteration, the composite of the two maps, $\gamma_l \cdot \varphi^{\perp}$, generates a series of figures $\boldsymbol{X}_i$ $(i = 0, 1, 2, \ldots)$ (thicker solid lines), each of which corresponds to a ternary RPH tiling. The limit figure $\boldsymbol{X}_{\infty}$ is the boundary of the atomic surface $\boldsymbol{W}$ for the RPH tiling generated solely by the left-handed GPSP. Note that a triangular region close to the boundary of $\boldsymbol{W}$ is divided into a central regular pentagon (A), 3/5 of which is occupied, and the two adjacent isosceles triangles (B), half of which in total is occupied.

a single GPSP iteration. The relevant right-eigenvectors are common to the two matrices, reading

$$\mathbf{v} = (\tau^3 - 4, \tfrac{1}{2}[1 + (1/\tau^2)], \tfrac{1}{2}[1 + (1/\tau^2)], 1, 1, 1)^t \doteqdot (0.236, 0.691, 0.691, 1, 1, 1)^t, \quad (5)$$

where the superscript t indicates the transposition. These six components provide the relative area (volume) of the tiles labelled a to f.

On the other hand, the left-eigenvectors for the common maximal eigenvalue τ^4 give the number ratio of the tiles. For $\boldsymbol{M}_1$ and $\boldsymbol{M}_2$, the relevant left-eigenvectors are

$$\mathbf{u}_1 = (\tau^4, \tau^3 + 1, 2\tau^3, \tau^3 - 1, 1, 0) \doteqdot (6.854, 5.236, 8.472, 3.236, 1, 0), \quad (6)$$

$$\mathbf{u}_2 = (\tau^4, \tau^3 - 1, 2\tau^3 + 2, \tau^3 - 1, 0, 1) \doteqdot (6.854, 3.236, 10.472, 3.236, 0, 1), \quad (7)$$

respectively. That the eigenvectors are different might seem troublesome if the two GPSPs are applied in an arbitrary order. It turns out, however, that no problem is caused by the difference, since the inflation matrices multiplied by the wrong eigenvectors will just give the right ones, *i.e.*,

$$\mathbf{u}_1\boldsymbol{M}_2 = \tau^4\mathbf{u}_2, \quad (8)$$

$$\mathbf{u}_2\boldsymbol{M}_1 = \tau^4\mathbf{u}_1. \quad (9)$$

It follows that the number ratios of the tiles depend only on the chiralities of the final two iterations. The above two distributions for the six types of tiles do not cause a difference in the number ratios of the three prototiles, since the sums over components for P tiles or H tiles are common to the two left-eigenvectors. It follows that the number ratios of the three prototiles in the present RPH tilings are $R : P : H = 1 : 2 : 1/\tau$, while the mean volume of the tiles is $1/\tau$ times that of an H tile.

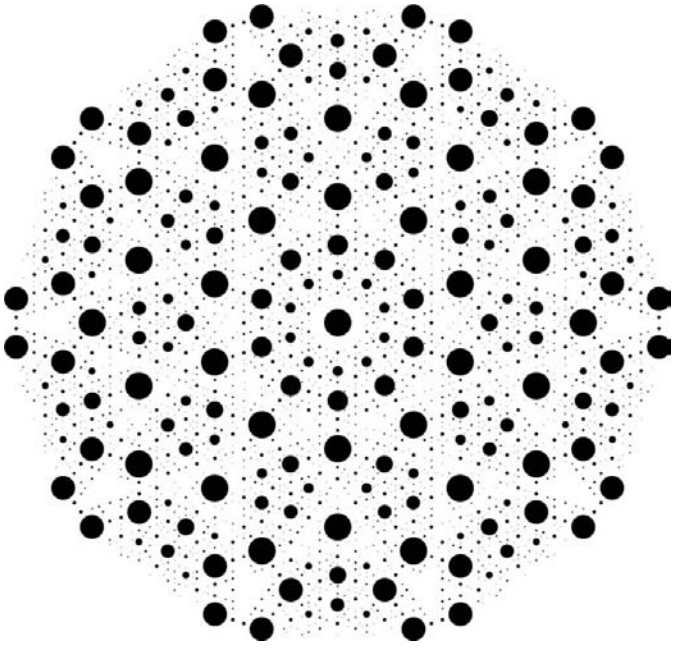

Figure 9
The structure factor of the RPH tiling generated by the left-handed GPSP depicted in Fig. 4. The area of each spot corresponds to the intensity. The chirality is manifested in the weakest spots.

The differences in the left-eigenvectors manifest themselves in the statistics of local arrangements of tiles in the relevant tilings. For instance, the second components of $\mathbf{u}_1$ and $\mathbf{u}_2$ representing the relative frequencies of P tiles labelled b are different. This is manifested in the frequencies of the local centres of fivefold symmetry in the two tilings shown in Fig. 5; the difference can be rather significant from the viewpoint of the structural stability as well as the physical properties if these tilings are to be used for modelling physical QCs. Importantly, the difference should also be connected to the boundary shapes of the atomic surfaces. This point, however, will be left for future investigation.[5] There are on the other hand three types of local centres of twofold symmetry (Niizeki, 1989*b*) located (i) at the centres of R tiles labelled a or $\overline{a}$, (ii) at the centres of H tiles labelled e, $\overline{e}$ or f, and (iii) at the mid-edge positions between two adjacent P tiles both labelled b. The frequencies of these twofold centres are common to the two cases.

7. Further remarks

The generality of the GPSP scheme is capable of generating a number of unknown quasiperiodic tilings, many of which are chiral. Let us briefly consider what the structure factor of a chiral tiling looks like. In our examples, the breaking of the mirror symmetry is carried by a small part of the atomic surface near the boundary, while the main body of the atomic surface maintains the mirror symmetry. Since the latter part provides the main contribution to the structure factor, the chirality is only manifested in relatively weak Bragg peaks. A structure factor is shown in Fig. 9 for the tiling shown in Fig. 5(*a*), assuming a point scatterer on every vertex.

In the GPSP scheme, the removal of unnecessary points from the given candidates for the point decoration forms a critical step. This makes the scheme the most general and robust technique for generating decagonal tilings. Furthermore, the application of the basic idea to the octagonal as well as the dodecagonal cases is straightforward. Indeed, for most of the known tilings, whether the atomic surfaces are polygonal or fractal, inflation rules can be rephrased as GPSPs, *i.e.* the combination of an expansion step and a point decoration step.

Let us consider the particular case of the dodecagonal square–triangle tilings. In this case, each of the vertices in the expanded tiling is decorated by a three-shell motif $\boldsymbol{S}$, comprising the origin, an inner hexagon and an outer dodecagon. The hexagon can take two different orientations, which can be chosen at random (Smith, 1993; Gähler, 1988) or according to a deterministic rule; for instance, the local coor-

[5] Identifying the classes of local centres of symmetry (Niizeki, 1989*b*) in quasiperiodic tilings is an important task, which has been addressed in a systematic way for the cases with polygonal atomic surfaces (Niizeki, 2007*b*). A generalized argument is hence necessary for handling the cases with fractal atomic surfaces.

dination can be used to fix the orientation (Hermisson *et al.*, 1997). One can see a similarity in the situation to the case of the decagonal tilings that are presented in this paper.

Different tilings that are generated by applying different GPSPs in different orders are all members of the random tiling ensemble with the same set of prototiles. They are likely to have energies very close to each other, so they have similar statistical weights. Since they form a deterministic subset of the relevant random tiling ensemble, the relevant contribution to the entropy is called the 'deterministic entropy', a term coined by Smith (1993).

Either of the left-handed and the right-handed GPSPs for the RPH tilings is defined by exclusively applying one of the two division rules for the T complex; see Fig. 3(*c*). One readily recognizes that these two division rules are mutually connected through a phason flip involving three tiles. Accordingly, the RPH tilings embrace an abundance of flipping sites. This has a significant implication when a physical realization of a similar structure is to be considered, since the phason degrees of freedom must play an important role in the structural stabilization. One should also bear in mind that the same kind of phason flips has been observed *in situ* in a *d*-Al—Cu—Co QC at a temperature of 1123 K with a transmission electron microscope (Edagawa *et al.*, 2000).

8. Conclusions

A general inflation scheme for generating decagonal quasiperiodic tilings has been proposed. In the new scheme, inflation rules comprise three steps: expansion with the ratio σ, decoration of every vertex by a finite motif $\boldsymbol{S}$ and elimination of unnecessary points by local rules. At every iteration, the resulting point set should be unit-connective and form the vertex set of a tiling. Since the point decoration process can be readily generalized, various new tilings are expected to be found. The usefulness of the present scheme has been demonstrated by generating several new decagonal tilings, among which the family of ternary tilings has been analysed in detail. The concept can be extended not only to the octagonal and dodecagonal cases, but also to the icosahedral cases (including P-, F- and I-type Bravais classes), for which only a few tilings are known.

The author is greatly indebted to K. Niizeki for instruction in the mathematics of quasilattices and for a comment on the issue of local centres of symmetries in the present tilings. The author is also grateful to M. Mihalkovič, T. Ogawa and A. Yamamoto for helpful comments on the subject.

References

Baake, M., Klitzing, R. & Schlottmann, M. (1992). *Physica A*, **191**, 554–558.
Baake, M. & Schlottmann, M. (1997). *Proceedings of the 5th International Conference on Quasicrystals*, edited by C. Janot & R. Mosseri, pp. 15–21. Singapore: World Scientific.
Baake, M., Schlottmann, M. & Jarvis, P. D. (1991). *J. Phys. A*, **24**, 4637–4654.
Beenker, F. P. M. (1982). Eindhoven University of Technology Report No. 82-WSK-04. Eindhoven, The Netherlands.
Bruijn, N. G. de (1981). *Ned. Akad. Wetensh. Proc. Ser. A*, **84**, 38–66.
Cockayne, E. (1994). *Phys. Rev. B*, **49**, 5896–5910.
Cockayne, E. (1995). *Phys. Rev. B*, **51**, 14958–14961.
Duneau, M. & Katz, A. (1985). *Phys. Rev. Lett.* **54**, 2688–2691.
Edagawa, K., Suzuki, K. & Takeuchi, S. (2000). *Phys. Rev. Lett.* **85**, 1674–1677.
Edagawa, K., Tamaru, H., Yamaguchi, S., Suzuki, K. & Takeuchi, S. (1994). *Phys. Rev. B*, **50**, 12413–12420.
Falconer, K. (1990). *Fractal Geometry*, pp. 113–118 (§§9.1 and 9.2). New York: Wiley.
Fujita, N. & Niizeki, K. (2008). *Philos. Mag.* **88**, 1913–1919.
Gähler, F. (1988). Doctoral dissertation, Swiss Federal Institute of Technology, Zürich, Switzerland.
Godrèche, C., Luck, J. M., Janner, A. & Janssen, T. (1993). *J. Phys. I France*, **3**, 1921–1939.
Grünbaum, B. & Shephard, G. C. (1987). *Tilings and Patterns*, ch. 10. New York: Freeman.
Hermisson, J., Richard, C. & Baake, M. (1997). *J. Phys. I France*, **7**, 1003–1018.
Hutchinson, J. E. (1981). *Indiana Univ. Math. J.* **30**, 713–747.
Kramer, P. & Neri, R. (1984). *Acta Cryst.* A**40**, 580–587.
Luck, J. M., Godrèche, C., Janner, A. & Janssen, T. (1993). *J. Phys. A Math. Gen.* **26**, 1951–1999.
Mackay, A. L. (1982). *Physica A*, **114**, 609–613.
Niizeki, K. (1989*a*). *J. Phys. A Math. Gen.* **22**, 193–204.
Niizeki, K. (1989*b*). *J. Phys. A Math. Gen.* **22**, 4281–4293.
Niizeki, K. (2007*a*). *Philos. Mag.* **87**, 2855–2861.
Niizeki, K. (2007*b*). *Philos. Mag.* **87**, 2863–2868.
Niizeki, K. (2008). *J. Phys. A Math. Theor.* **41**, 175208.
Papadopolos, Z. & Kasner, G. (2003). *Coverings of Discrete Quasiperiodic Sets*, edited by P. Kramer & Z. Papadopolos, §5.2. Berlin: Springer.
Penrose, R. (1974). *Bull. Inst. Math. Appl.* **10**, 266–271.
Penrose, R. (1978). *Eureka*, **39**, 16–22.
Penrose, R. (1979). *Math. Int.* **2**, 32–37.
Shechtman, D., Blech, I., Gratias, D. & Cahn, J. W. (1984). *Phys. Rev. Lett.* **53**, 1951–1953.
Smith, A. P. (1993). *J. Non-Cryst. Solids*, **153&154**, 258–263.
Stampfli, P. (1986). *Helv. Phys. Acta*, **59**, 1260–1263.
Yamamoto, A. (1996). *Acta Cryst.* A**52**, 509–560.
Zobetz, E. (1992). *Acta Cryst.* A**48**, 328–335.